PCCP

PAPER

View Article Online
View Journal | View Issue

Cite this: *Phys. Chem. Chem. Phys.*, 2019, **21**, 2771

Understanding charge carrier dynamics in a P3HT:FLR blend†

Jessica Patel, ‡[a] Abhishek Sharma,‡[bc] Mihirsinh Chauhan, [d] Md. Aatif,[bc] Nikita Vashistha,[e] Mahesh Kumar,[e] Brijesh Tripathi, [a] Suresh Chand,[bc] J. P. Tiwari *[bc] and Manoj Kumar Pandey *[a]

Received 31st August 2018,
Accepted 7th January 2019

DOI: 10.1039/c8cp05518a

rsc.li/pccp

In organic semiconductors, optical absorption is pivotal for the performance of optoelectronic devices. The absorption by the semiconductors generates excitons which dissociate into free charge carriers, resulting in energy conversion. Although high performance has been achieved in non-fullerene organic solar cells, their charge generation behavior is far from being well understood. Keeping this in view, we have employed optical spectroscopic tools to study the charge generation mechanism in FLR (1,6,7,10-tetramethylfluoranthene) as a non-fullerene electron acceptor blended with P3HT (poly(3-hexylthiophene)) as an electron donor in five different solvents. Through steady state UV-visible and photoluminescence spectroscopy, we provide a basic understanding of charge transport by enlightening the influence of solvents on the aggregation behavior and exciton bandwidth. Furthermore, for the first time, by employing ultrafast vis-NIR transient absorption spectroscopy, we address the ultrafast charge generation and charge separation mechanism with systematic variation in solvent polarity by incorporating the time evolution of the transient species under various pump–probe wavelengths in the range of 450 nm to 1600 nm. For the different excitation wavelengths, the lifetime kinetics have been depicted by their multiexponential fits. The results show a fast decay term at a lifetime of a few picoseconds (ps) (~1 to 5 ps) and a slow decay term at a lifetime of ~500 ps. The charge generation in the P3HT:FLR blend proceeds on a ps time scale, which implies good intermixing of the components. It is clearly established that the non-halogenated solvents influence this aggregation behavior and higher conjugation lengths with higher photoluminescence quenching contribute to the higher charge generation. The enhanced polaron population in P3HT with the addition of FLR illustrates the importance of this acceptor material in the blend because a good solvent-material combination is essential to enhance the charge generation. As such, this comprehensive study explicitly shows the role of FLR as an emerging efficient non-fullerene acceptor for further improving the performance of devices.

Introduction

In organic solar cells (OSCs), two vertically stacked donor:acceptor (D:A) materials are chosen to absorb light in a broad solar spectrum; this is followed by splitting of excitons into free charge carriers at the D:A interface, which finally leads to charge transport and charge collection at the respective electrodes for generation of electricity. Conventionally, in OSCs, a solution of a conjugated polymer as D and a fullerene as A is spin-coated on the back of the electrode, which results in the formation of the active layer. Due to their three-dimensional electron transport properties, high electron affinity, high electron mobility and formation of favorable blend morphologies with donors, fullerenes have been the most commonly used acceptors to date.[1–3] However, the challenges of fullerenes, such as poor absorption in the visible region,[4] high synthetic cost,[5] and energy level tunability,[6] have encouraged researchers to develop

[a] *Department of Science, School of Technology, Pandit Deendayal Petroleum University, Gandhinagar 382007, India. E-mail: manoj.pandey@sot.pdpu.ac.in; Tel: +91 79 2327 5227*
[b] *Advanced Materials and Devices Division (FOED Group), CSIR-National Physical Laboratory, New Delhi 110012, India*
[c] *Academy of Scientific and Innovative Research (AcSIR), CSIR-National Physical Laboratory, Dr K. S. Krishnan Marg, New Delhi 110012, India. E-mail: jai_ti2002@yahoo.com, tiwarijp@mail.nplindia.org; Tel: +91 79 2327 5455, +91 11 45608640*
[d] *Department of Solar Energy, School of Technology, Pandit Deendayal Petroleum University, Gandhinagar-382007, India*
[e] *Ultrafast Optoelectronics and Terahertz Photonics Lab, Advanced Materials and Devices Division, National Physical Laboratory, New Delhi-110012, India*

† Electronic supplementary information (ESI) available. See DOI: 10.1039/c8cp05518a

‡ These authors contributed equally.

non-fullerene acceptors (NFAs) which can be synthetically modified to increase their absorption ranges by tuning their highest occupied molecular orbitals (HOMO) and lowest unoccupied molecular orbitals (LUMO).[7–9] A fundamental understanding of the electronic interaction between D and A enables control of the active layer morphology, which facilitates maximum charge extraction with balanced phase separation.[10–12] To optimize the charge separation at the D:A interface, a suitable conjugation length with the appropriate π–π^* transitions is required. Many studies have been reported to explore the sensitivity of blend morphologies by choosing suitable processing solvents,[13–15] solvent additives[16,17] and annealing conditions (thermal, solvent).[18–20] Halogenated solvents are employed as processing solvents in OSCs[13,21] because they exhibit bi-continuous morphologies due to their high solubility. However, non-halogenated solvents are preferential due to environmental concerns and their facile processability in large-scale manufacturing.[22–24] Therefore, current R&D efforts are focused on the development of non-halogenated solvents with similar functionalities to halogenated solvents.

Keeping the above in view, several morphological tools were employed to study the D:A nano-morphology in solution as well as in films using transmission electron microscopy (TEM),[25–27] atomic force microscopy (AFM)[28] and grazing incidence X-ray diffraction (GIXD).[29] These tools are used to study the bicontinuous phase separation, determination of the accurate domain size and interdomain correlation, which are relevant to the charge transport mechanism. However, spectroscopic measurements such as steady state UV-visible and photoluminescence (PL) spectroscopy are useful to evaluate the exciton generation and dissociation into free charge carriers.[30,31] Because the absorption of photons and the generation of free charge carriers are different in solutions and in films, these spectroscopic tools provide useful information for studying the aggregation behavior. Ordered and disordered aggregates affect the charge transfer (CT) kinetics. In the study of CT kinetics, transient absorption spectroscopy (TAS) is a widely used technique which is crucial for demonstrating rapid and efficient charge generation in OSCs.[32,33] The charge generation at the D:A interface can be defined by two processes: (a) exciton delocalization[34] at the ultrafast component of <100 fs and (b) exciton diffusion at picosecond timescales.[35] Through these processes, the population of free charge carriers becomes an important factor in defining the optical and morphological relationships.[36–38] Thus, analyzing these signals is necessary to understand the charge generation in OSCs.

To demonstrate this concept, we used a spectroscopic approach for a blend system consisting of newly developed 1,6,7,10-tetramethylfluoranthene (FLR) as an electron acceptor and P3HT as an electron donor in different halogenated and non-halogenated solvents. FLR, the smallest fragment of fullerene, was previously reported as a non-fullerene acceptor in OSCs by our group.[39] Several other fluoranthene core-based derivatives have been actively reported in organic light emitting diodes (OLEDs),[40,41] organic field effect transistors (OFETs)[42–44] and OSCs.[45,46] Recently, some of these derivatives have also been used as dopant-free hole transporting layers in perovskite solar cells.[47] These reports indicate the importance of this class of materials in a wide range of applications. In our studies, we focus on the fundamental principles of photophysics, such as charge generation and charge separation, for the P3HT:FLR blend system, to determine the ability of FLR as an acceptor. Firstly, through steady-state UV-visible and photoluminescence studies, one can understand the aggregation behavior and analyze the influence of aggregates on the charge transfer from D to A. Vis-NIR transient absorption (TA) spectroscopy allows us to monitor the process of charge generation in the P3HT:FLR blend system with the influence of solvent at room temperature. For the P3HT:FLR blend system, the charge generation dynamics drastically change in halogenated and non-halogenated solvents. For all the solvents, we observed the creation of singlet excitons that eventually dissociated into polarons. It can be observed that the polaron formation is enhanced significantly with the addition of FLR as an acceptor. Further, it was observed that non-halogenated solvents are more favorable for increased yields of polarons on an ultrafast time scale. This is clearly depicted by kinetics studies, wherein it can be seen that efficient free charge carrier generation in P3HT:FLR is enhanced using non-halogenated solvents.

Experimental methods

Materials

1,6,7,10-Tetramethylfluoranthene (FLR) was synthesized as per our previous report.[39] Poly(3-hexylthiophene) (P3HT) and the solvents under study, namely chloroform (CF), 1,2-dichlorobenzene (ODCB), chlorobenzene (CB), *o*-xylene (XYL) and tetrahydrofuran (THF), were purchased from Sigma Aldrich and Merck.

Optical measurements

The absorption spectra were obtained using a Shimadzu 2401 PC instrument, and photoluminescence spectroscopy was carried out using a Fluorolog system (Jobin Yvon-Horiba, model-3-11).

Femtosecond transient absorption spectroscopy

This study was performed using an experimental setup consisting of an oscillator (Micra by Coherent), amplifier (Legend by Coherent), OPA (by Light Conversion) and spectroscopy system (Helios by Ultrafast Systems). The 4 mJ output of the amplifier with a pulse width of 35 fs centered at 800 nm was split into two parts. One part was fed to the OPA with 1.8 mJ energy, and the other part with 0.5 mJ energy was fed to the spectrometer with a delay stage of 0 to 8 ns. Broadband white light was generated inside the spectrometer by passing the split beam through a sapphire plate which is capable of generating probe pulses of 350 to 850 nm. A highly stable OPA output of 425 nm was selected as the pump beam with a fluence of 16 $\mu J\ cm^2$ for the P3HT and P3HT:FLR samples. An OPA output of 350 nm with same fluence energy was selected as the pump wavelength for the FLR sample. Surface Xplorer software and Origin 9.1 were used for the analysis and kinetics fitting.

Sample preparation

Pristine P3HT solutions in different solvents were prepared with concentrations of 1 mg ml^{-1}. The pristine FLR solution in THF solvent was prepared with a concentration of 6 mg ml^{-1}. The P3HT : FLR (1 : 6) blend was prepared by blending individual components in these solvents with a concentration of 7 mg ml^{-1}. The blend ratio for P3HT : FLR was 1 : 6 as per our previous work.[39]

Morphological characterization

The surface morphologies were measured by atomic force microscopy (AFM) using a Solver P47-PRO SPM instrument.

Results and discussion

Optical spectra and photophysics of pure P3HT, pure FLR and the P3HT:FLR blend system

The molecular structures of P3HT and FLR as an electron donor and electron acceptor, respectively, with their corresponding energy levels are shown in Fig. 1. The structures of the halogenated solvents, namely chloroform (CF), chlorobenzene (CB), 1,2-dichlorobenzene (ODCB), and non-halogenated solvents, namely *o*-xylene (XYL) and tetrahydrofuran (THF), are also shown in this figure. These solvents have different polarities, which influences the absorption and emission spectra of the pristine compounds as well as the blend system.[48] Halogenated solvents are exclusively used in OSCs according to the literature that has been published in recent years. The use of high-boiling-point halogenated solvents is related to their ability to dissolve conjugated polymers; they tend to dry slowly and have superior film-forming properties.[49–51] However, due to their limitations of toxicity to the environment and humans[52] and recent evidence of device instability,[53] researchers are focusing on the use of non-halogenated solvents. These solvents have low boiling points, with similar solubilities and film forming properties to those of halogenated solvents. Interesting variations were observed by comparing halogenated solvents and non-halogenated solvents; Table S1 (ESI†) shows the boiling points and polarities of the solvents considered in this study.

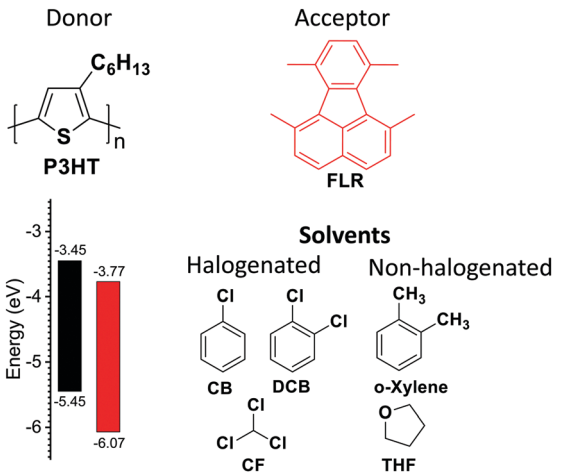

Fig. 1 Molecular structures of the donor and acceptor molecules with their corresponding energy levels and the different solvents used in this study.

The absorption spectra of pristine P3HT in these solvents are shown in Fig. S1 (ESI†). For pristine P3HT in halogenated solvents, only one distinct 0–1 transition peak was observed at 2.8 eV. Compared to CF, there was a bathochromic shift in CB and ODCB to ~2.7 eV. Similarly, for the non-halogenated solvents, THF and XYL showed the 0–1 peak, but a weak peak appeared at 2.1 eV for XYL alone; this was attributed to the 0–0 transition in P3HT. To observe the influence of different solvents on the P3HT:FLR blend system, we measured the absorptions, as shown in Fig. 2a. It was clearly observed that the absorption spectrum of the blended solution is the superposition of the single components, as expected from the BHJ results, as shown by the characteristic transition peaks in solution phase at 3.68 eV, 3.33 eV, 3.18 eV for FLR[39] and at 2.77 eV and 2.06 eV for P3HT.[54]

The P3HT thin film undergoes intermolecular interactions which can form phases with short-range or long-range order. These ordered chains are commonly referred to as aggregates. The formed aggregates have effects on the photophysical and morphological properties which are prerequisites for semiconducting devices.[51,55,56] The boiling point of the solvent, the solubility parameter of the solvent and the side chains of the film influence the aggregation behavior.[57,58] Therefore, it is necessary to study the aggregation behavior of the P3HT:FLR blend to understand its morphological and photo-physical aspects. We measured the absorption spectra for solutions as well as thin films. To study the aggregation behavior of the P3HT:FLR blend, we will consider the transition peaks of 0–0 and 0–1. In the solution phase, for all the solvents, the blend system showed only one 0–1 transition at ~2.7 eV; however, for XYL, a weak 0–0 peak appeared. In the thin films, both 0–0 and 0–1 transition peaks were observed. For the halogenated solvents, the intensity of the 0–0 peak distinctly increased with increasing boiling point of the solvent in the order of CF < CB < ODCB for the thin films. A slow evaporation rate is required for distinct peaks at 2 eV. For non-halogenated solvents, only XYL showed pre-aggregation behavior in the blend solution. The interesting results achieved in XYL were attributed to greater aggregation with a faster evaporation rate than ODCB. In thin films, for THF (boiling point similar to $CHCl_3$), we achieved less aggregation compared to XYL, as is evident from the blue shift at ~2.8 eV (as shown in Fig. S1, ESI†). This blue shift indicates that no aggregation occurred in the polymer backbone for THF.

Fig. 2b shows the changes in the aggregation in different solvents, which can be attributed to the ordered–disordered transitions when going from solution to thin film. In the spectra, the featureless and broad peak at 2.75 eV can be attributed to disordered chain formation. As observed from the spectra, the intensity of the 0–0 transition peak increased in the order CF < THF < CB < ODCB < XYL for the P3HT:FLR blend. This increase is due to planarization of the disordered chains, which is due to an increase in conjugation length.[59]

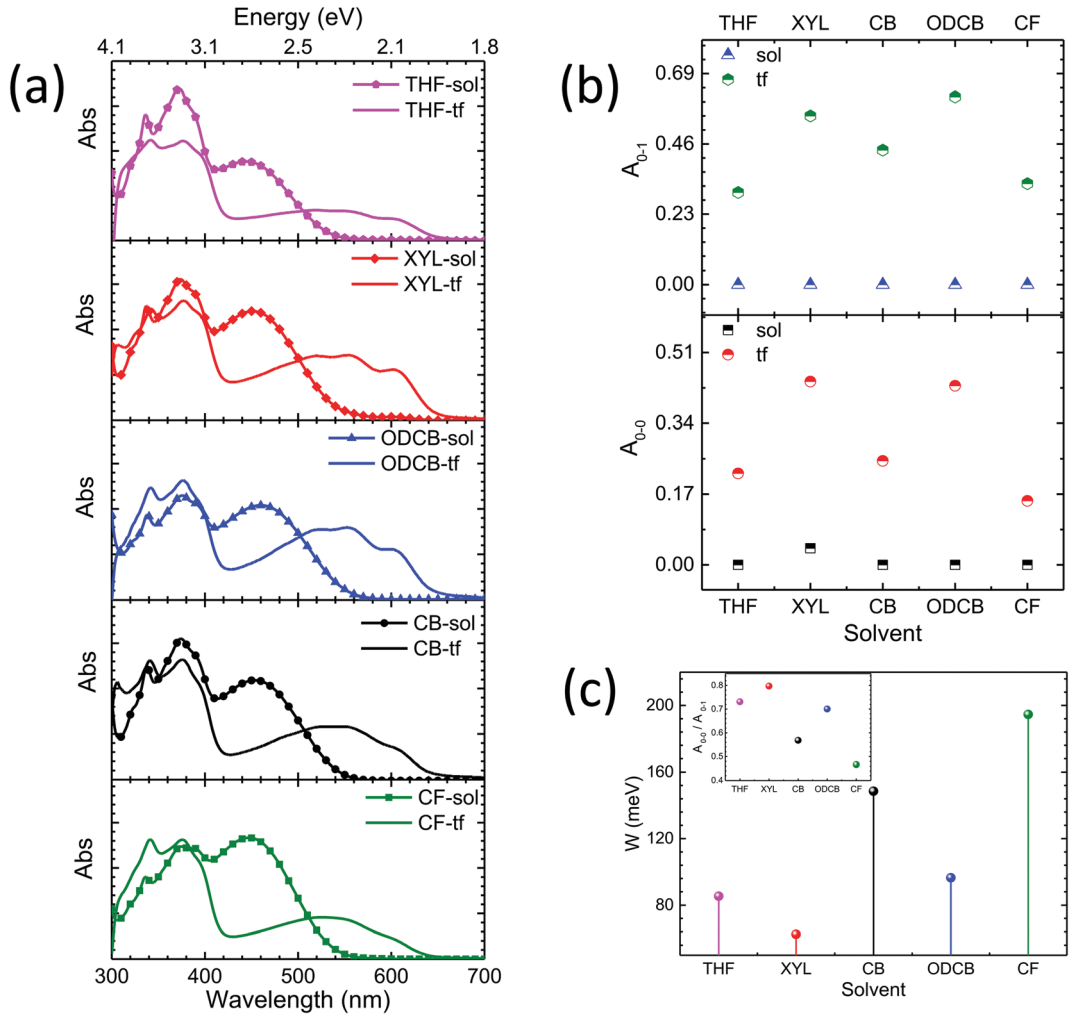

Fig. 2 (a) Absorption spectra of the P3HT:FLR blend in halogenated and non-halogenated solvents. (b) Intensities of A_{0-0} and A_{0-1} with respect to solvent in solution and in thin films. (c) Exciton bandwidth as a function of solvent type, with the inset showing the ratios of A_{0-0}/A_{0-1}.

The conjugation length increases from the disordered phase to longer repeat units in the aggregated phase, which can be correlated to the exciton bandwidths obtained from the spectra. The free exciton bandwidths (W) can be calculated from the UV spectra using eqn (1):[60,61]

$$\frac{A_{0-0}}{A_{0-1}} = \left(\frac{1 - 0.24W/E_p}{1 + 0.073W/E_p}\right) \quad (1)$$

where A_{0-0} and A_{0-1} are the peak absorbances from Fig. 2a and E_p is the intermolecular vibrational energy, maintained as 0.179 eV.[62] A plot of W as a function of solvent is shown in Fig. 2c. The conjugation length and size of the aggregates determines the magnitude of W, which is inversely proportional to the conjugation length and proportional to the degree of disorder. From Fig. 2c, it can be observed that W decreases in the order CF > CB > ODCB > THF > XYL; the inset shows the ratios of A_{0-0} and A_{0-1}. In the active layer of crystalline P3HT, W is proportional to the nearest neighbor excitonic interaction. This neighboring interaction decreases with increasing conjugation length of the polymer chain.[63] The smallest W exhibited in XYL can be attributed to a longer conjugation length, which is consistent with the highest phase purity and red-shifted absorption peak at ~2.73 eV. As the conjugation length increases, the optical gap decreases due to the stronger intrachain coupling between the neighbor thiophene rings, causing the red-shift. This bathochromic shift indicates that the dipole moment is higher in the excited state than in the ground state, which implies that the excited state is more sensitive than the ground state. W also provides information about the width of the Gaussian distribution of the density of localized states, which serve as carrier traps at the HOMO–LUMO levels.[64] This suggests that P3HT:FLR in CF solvent has the deepest distribution of traps, whereas XYL and THF have shallow distributions. As the distribution of localized states deepens, the charge carriers are more likely to become trapped and recombine. Thus, a higher W is indicative of higher free charge carrier recombination.

The photoluminescence (PL) after photoexcitation was observed for the pristine P3HT and P3HT:FLR blends in different solvents, as shown in Fig. 3. The PL features of the blend system are similar

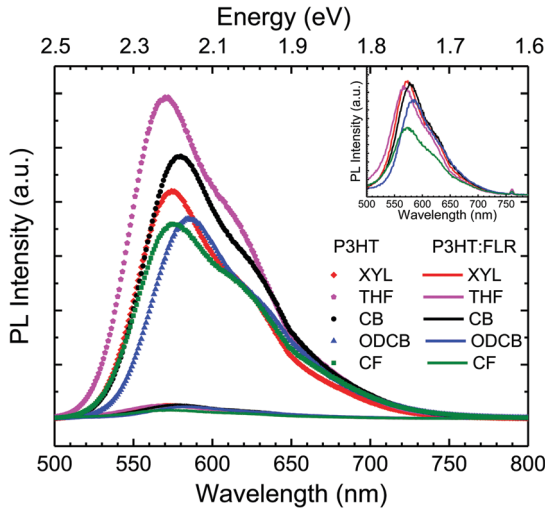

Fig. 3 Photoluminescence spectra of the P3HT:FLR blend solutions in different solvents; the inset shows zoomed-in spectra of the quenched blend.

to the donor P3HT emission, which indicates that energy transfer occurs from the electron acceptor FLR to the electron donor P3HT. The PL spectra arise from the longest polymer segments after relaxation of the initial photoexcitation. In CF solvent, two emission peaks are observed in both the pristine and blended systems. As correlated with W, the shorter conjugation length in CF solvent is attributed to the random coil conformation. For other solvents, the red-shifts observed in the absorption spectra demonstrate absorption by the planar, aggregated chains.[65] Similarly, the corresponding PL spectra contain vibronic structures with peaks at 2.1 eV and 1.99 eV; these are mainly attributed to the C=C symmetric stretching mode at $\sim$1446 cm^{-1}, which can be well correlated with the FTIR spectra of the P3HT:FLR blend system, as shown in Fig. S3 (ESI†). The bathochromic shifts in the PL spectra for the other solvents compared to THF show the formation of more aggregated structures, as observed in the aggregation peaks (Fig. 2b). Compared to pristine P3HT, effective quenching is observed when P3HT is blended with FLR, which is attributed to increased exciton dissociation into electrons and holes. To calculate the relative quenching efficiencies (Q), eqn (2)[66] was used:

$$Q = 1 - \frac{\int \mathrm{PL}_{\mathrm{quencher}} \mathrm{d}\lambda}{\mathrm{PL}_{\mathrm{pristine}} \mathrm{d}\lambda} \qquad (2)$$

It can be seen that the highest relative quenching efficiency (Q) of 96% was observed for THF and CF. However, because the high W in CF indicates greater charge recombination possibility, THF is an appropriate choice to consider the higher Q value. XYL also shows a high Q value of 94%. Similarly, CB and ODCB have Q values of 95% and 94%, respectively. To deepen our understanding of the charge generation and exciton dynamics, transient absorption spectroscopy was performed.

Transient absorption (TA) spectroscopy

The systematic variation using different solvents and the detailed analysis of the blend system enable the study of the excitation which occurs after illumination. To study the primary photo-excitations and the photovoltaic conversion processes in the P3HT:FLR blend system, we performed ultrafast pump–probe transient absorption (TA) spectroscopy. The vis-NIR TA spectra of the blend were recorded with a low excitation fluence of 16 μJ cm^{-2} at 425 nm. Similarly, for pristine FLR, the spectra were recorded with an excitation fluence of the same energy at 340 nm. We specifically used the same fluence energy for the blend and P3HT to simplify interpretation of the data and to enable neglect of the effects due to the energy transfer from FLR to P3HT. This study was designed to enable comparison between pristine P3HT, pristine FLR and the P3HT:FLR blend system in THF under the same experimental conditions, as shown in Fig. 4.

In the TA spectra, the negative optical density (ΔOD) signals in the spectral region between 450 to 500 nm occur due to ground state bleaching (GSB), which is attributed to P3HT absorption. The spectral regions between 525 and 620 nm and 400 and 525 nm occur due to stimulated emission (SE) for P3HT and FLR, respectively, as shown in Fig. 4a and b. These regions arise from the pristine P3HT and FLR absorption and emission spectra, respectively, which is explained in the ESI† (Fig. S4). The difference in the GSB regions for FLR and P3HT arises due to the energetic separation of their absorption onsets (shown in Fig. 1). The TA spectra of P3HT:FLR (Fig. 4c) and the kinetics studies in the NIR region at 1000 nm (Fig. 4d) for pristine P3HT and FLR and their blend elucidate their interfacial charge dynamics. Compared to pristine FLR, the singlet exciton decay lifetime in the blend is shorter, showing efficient dissociation of excitons due to better quenching, as explained in the photoluminescence spectra (shown in Fig. 3).[67] Furthermore, to compare the effects of the different solvents on the charge generation and separation dynamics, detailed investigations of individual P3HT and the P3HT:FLR system were carried out.

Exciton dynamics of P3HT

To understand the TA data in the P3HT:FLR blend system, first, it is necessary to examine the exciton dynamics in pristine P3HT. The influence of solvent polarity on the charge generation in P3HT can be observed from the P3HT excitons. After determining the exciton dynamics, one can estimate the exciton-to-charge conversion in the P3HT:FLR blend system. Aggregation of P3HT has shown to affect its charge transport properties,[68] with an increase in hole mobility when it is blended with PCBM. The aggregation also affects the excited state of P3HT because the random placement of side chains disrupts the formation of ordered lamellae.[69,70] The exciton density is an important parameter to study because higher exciton densities cause decay mechanisms.[71] The choice of low fluence energy aids minimization of the excitation dynamics caused by second order effects.

Fig. 5 shows the TA spectra of pristine P3HT in the different solvents under study. Spectra acquired at pump–probe delay times of 5 ps, 100 ps, and 5 ns are shown. For CF and ODCB, at early times, the GSB region shows higher densities and

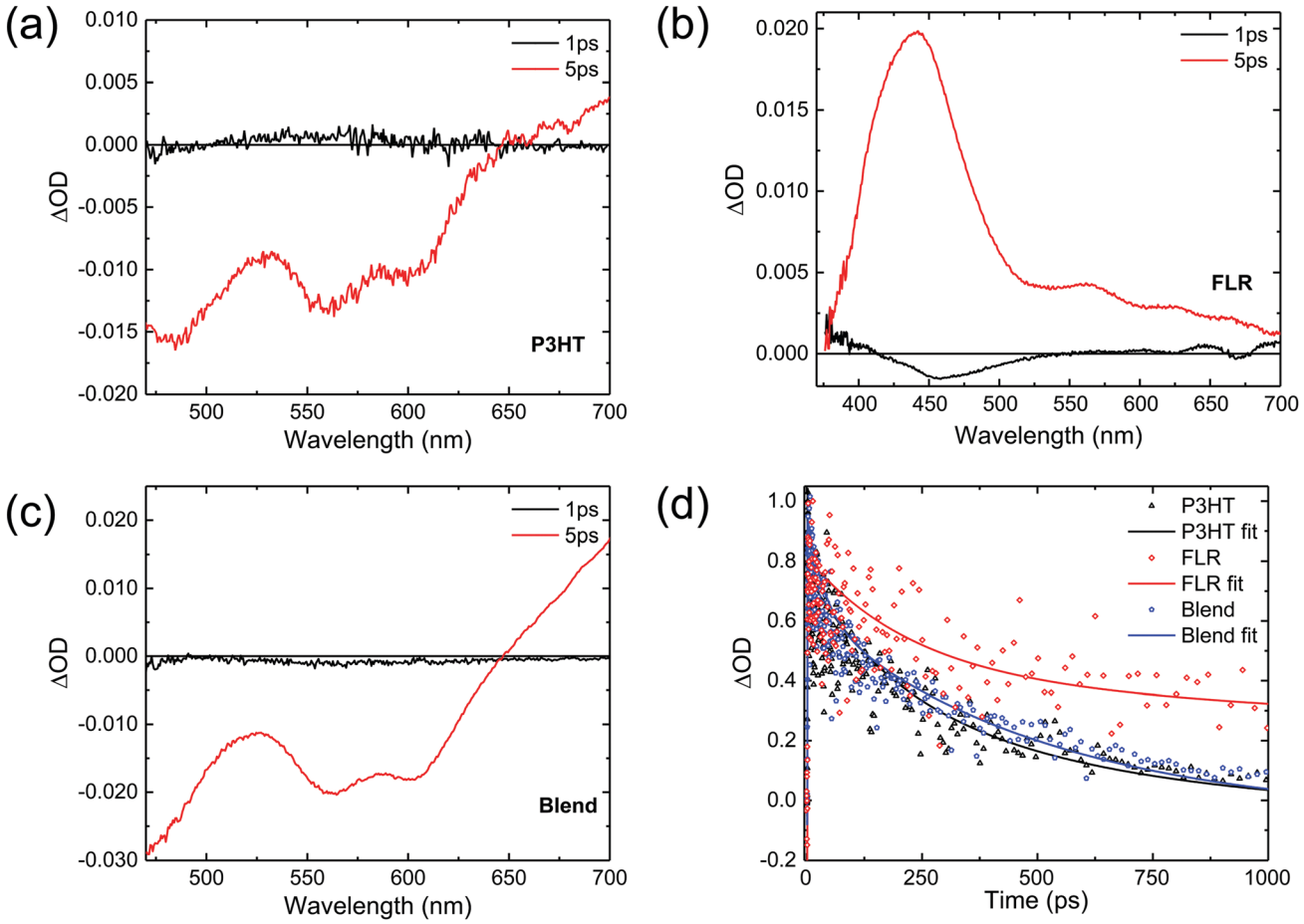

Fig. 4 TA spectra at 1 ps and 5 ps of (a) pristine P3HT, (b) FLR, and (c) the P3HT:FLR blend in THF and (d) kinetic curves of pristine P3HT, pristine FLR and the P3HT:FLR blend probed at 1000 nm to study the singlet exciton formation.

decreases with increasing delay time. However, for the other solvents, the GSB feature is consistent. This GSB feature corresponds to the absorption transitions of P3HT. This region shows that the P3HT chains are not in their ground state and represents the density of charge carriers present at that particular delay time. Thus, the photoexcitation of excitons and polarons decreases with longer delay times for CF and ODCB but remains almost constant for the other solvents. At early times, the presence of a significant SE feature at the wavelength of ~600 nm corresponds to the photoluminescence spectrum of P3HT. The prominent peak at 640 nm is attributed to the population of charge pairs which are directly photogenerated.[72] The SE of P3HT in halogenated solvents indicates the vibronic structures of the 0–0 transitions, with no vibronic structure for aggregation at shorter timescales. The 0–1 transitions appear at higher time scales for the non-halogenated solvents, which suggests that the ground state of the coiled chains recovers faster than the ground state of the aggregated chains by the energy transfer from the coiled chains to the aggregated chains.[61] The SE spectrum of P3HT arises from the superposition of the contributions of coils (around 500 to 550 nm) and aggregates (around 600 nm). In the aggregate absorption spectra, the high 0–0 peak signal indicates planar chains with long conjugation lengths and weak excitonic coupling to their neighbors. On the other hand, the lower 0–0 peak indicates chains with shorter conjugation lengths and stronger excitonic coupling.[61] However, the spectra for P3HT in non-halogenated solvents show the characteristic vibronic structure of the aggregates and show spectral shifts during the delay times studied in the TA measurements. XYL solvent shows the 0–0 peak, which is attributed to good P3HT ordering.[60] We observed a change in the ratio between the 0–0 and 0–1 SE peaks with time. This indicates that efficient energy transfer occurs from the coiled chains to the aggregated chains. The position of the SE peaks red-shifted slightly over higher delay times; the loss of SE can be attributed to an increase in the number of delocalized excitons.[73] The red-shift of the SE features shows the movement of excitons towards the ordered sites, and this can be studied by the lifetimes of the integrated kinetics. It is useful to analyze the excitation dynamics in the P3HT:FLR blend system to correlate the charge transfer time with the efficiency of exciton charging.

The positive signals in the NIR region from 830 nm to 1400 nm are due to photo-induced absorption (PIA), such as polarons and singlet excitons, respectively. The shape and intensity of the PIA feature changed with changing polarity of the solvent.[74] For the singlet exciton feature in the NIR region,

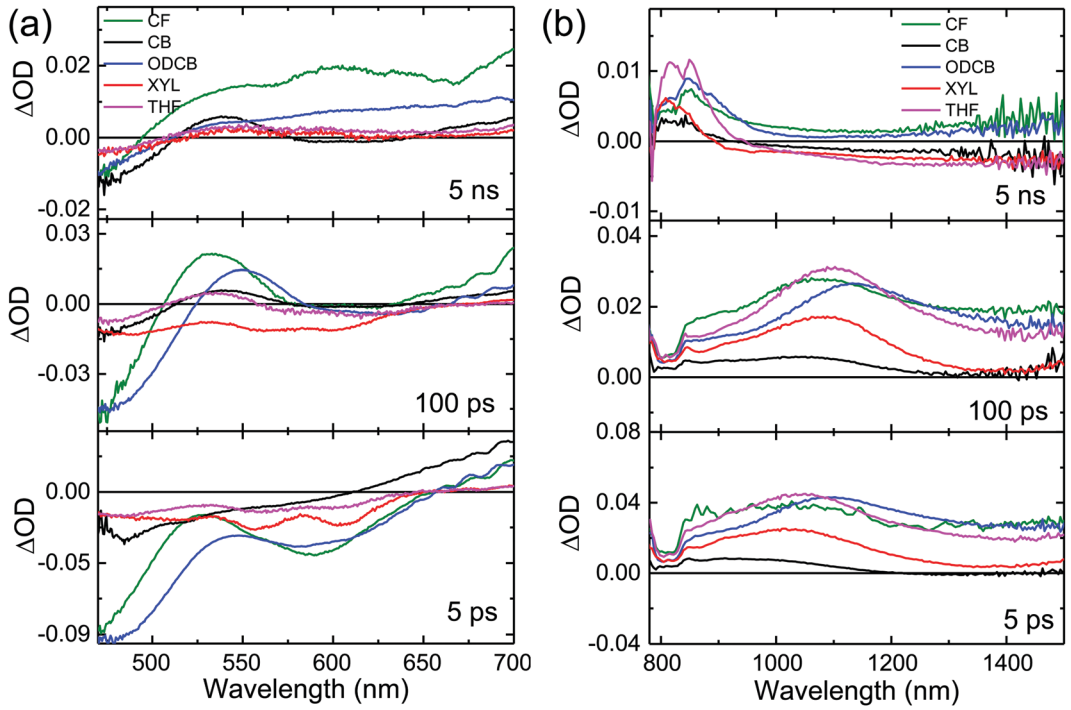

Fig. 5 Transient absorption (TA) spectra of P3HT in different solvents for 5 ps, 100 ps and 5 ns in (a) the visible region; (b) the NIR region.

it was observed that with increasing time, the density of singlet excitons decreased for all the solvents. A distinct peak at 820 nm was observed at 5 ns delay time, which is attributed to the P3HT triplet state. This arises due to intersystem crossing (ISC) from singlet excitons to triplet excitons.[75,76]

Charge transfer in the P3HT:FLR blend system

Fig. 6 shows the vis-NIR TA spectra of the P3HT:FLR blend system in the different solvents used in this study. The introduction of FLR results in an additional decay channel for photoexcitation, wherein charge separation occurs at the interface

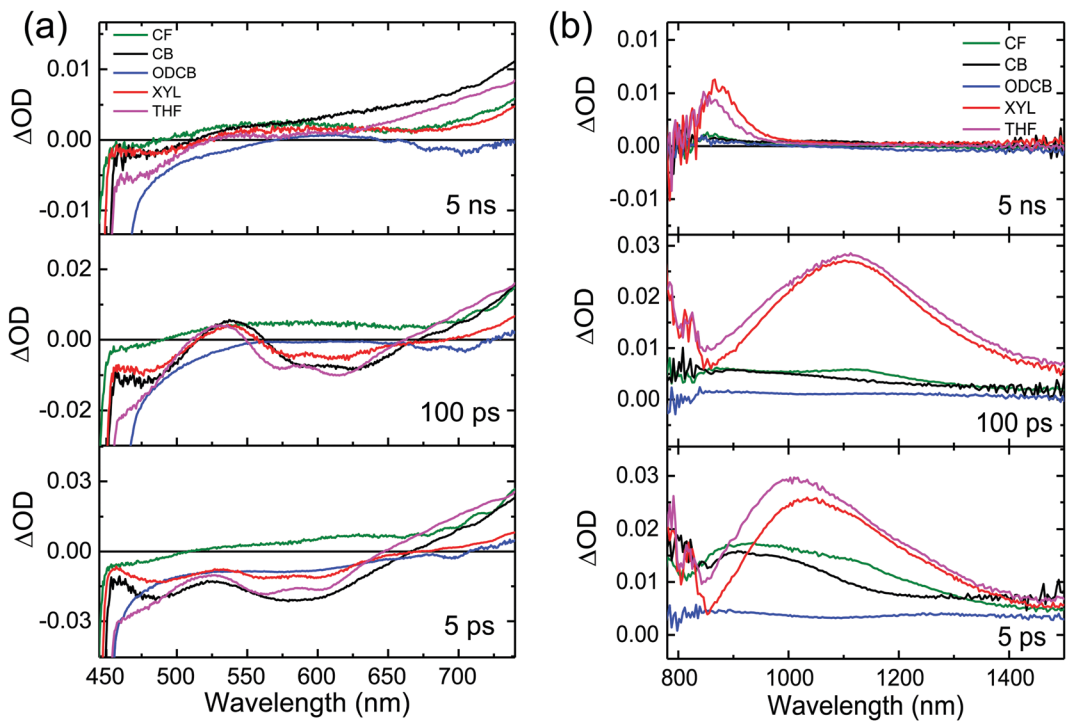

Fig. 6 Transient absorption (TA) spectra of P3HT:FLR in different solvents for 5 ps, 100 ps and 5 ns in (a) the visible region; (b) the NIR region.

followed by charge extraction or recombination. This will convert the P3HT exciton into a positive P3HT polaron, which is expected to produce a change in the TA spectra. The evolution of TA from excitonic to polaronic provides the rate of exciton diffusion to the heterojunctions and consecutive electron transfer. A similar trend to that observed for the pristine P3HT can be observed in the GSB, SE and PIA regions for the P3HT:FLR blend system, showing electron transfer from the donor to the acceptor in this case (Fig. 6a). At early times, the spectra consist of a GSB region corresponding to the absorption spectra of the blend (as shown in Fig. 2a). For CF and ODCB, the SE region is absent; however, it is clearly seen in other solvents. A change was observed in the SE region for non-halogenated solvents from a high intensity 0–0 peak at 100 ps to a low intensity peak at 5 ns, which implies that the excitation is initially delocalized and is then localized. This change may be due to spectral diffusion to more conjugated chain segments, to structural rearrangements of the polymer chains, or to a combination of both.[77] There is an absence of intensity of the 0–0 transition of GSB, which indicates that in the planar chain segments, the holes are not occupied, and the presence of FLR disrupts the ordered aggregates. The PIA region is consistent for all the solvents up to higher time scales, which implies that the addition of FLR to P3HT results in generation of additional P3HT cations, namely polarons.

A detailed analysis of these ultrafast electron processes can be obtained from the kinetics of the P3HT:FLR blend in different solvents. We thus observed the TA absorption profiles in the range of 900 nm to 1400 nm. In this range, the polaron absorption spectra match well with the reported P3HT spectra.[78] This region is assigned to absorption by singlet excitons, with a distinct transition at 1100 nm. These excitons then lead to stimulated emission and intersystem crossing due to the P3HT triplet state, with the characteristic transition at ~820 nm observed at 5 ns. This implies that exciton dissociation occurs on the polymer chains. At different delay times, we observed peaks in the range of ~850 nm to ~1200 nm, indicating polaronic and excitonic peaks, respectively.[79,80] In XYL and THF, the polaron intensity is higher than in other solvents (compared with pristine P3HT), showing the dissociation of singlet excitons into the polaron formation. Similar studies were carried out by Heeger's group[81] for P3HT-OH and P3HT-PCB systems in a non-halogenated solvent. Thus, it can be concluded that ultrafast electron transfer occurs from P3HT to FLR in XYL and THF solvents compared to halogenated solvents at these probe wavelengths.

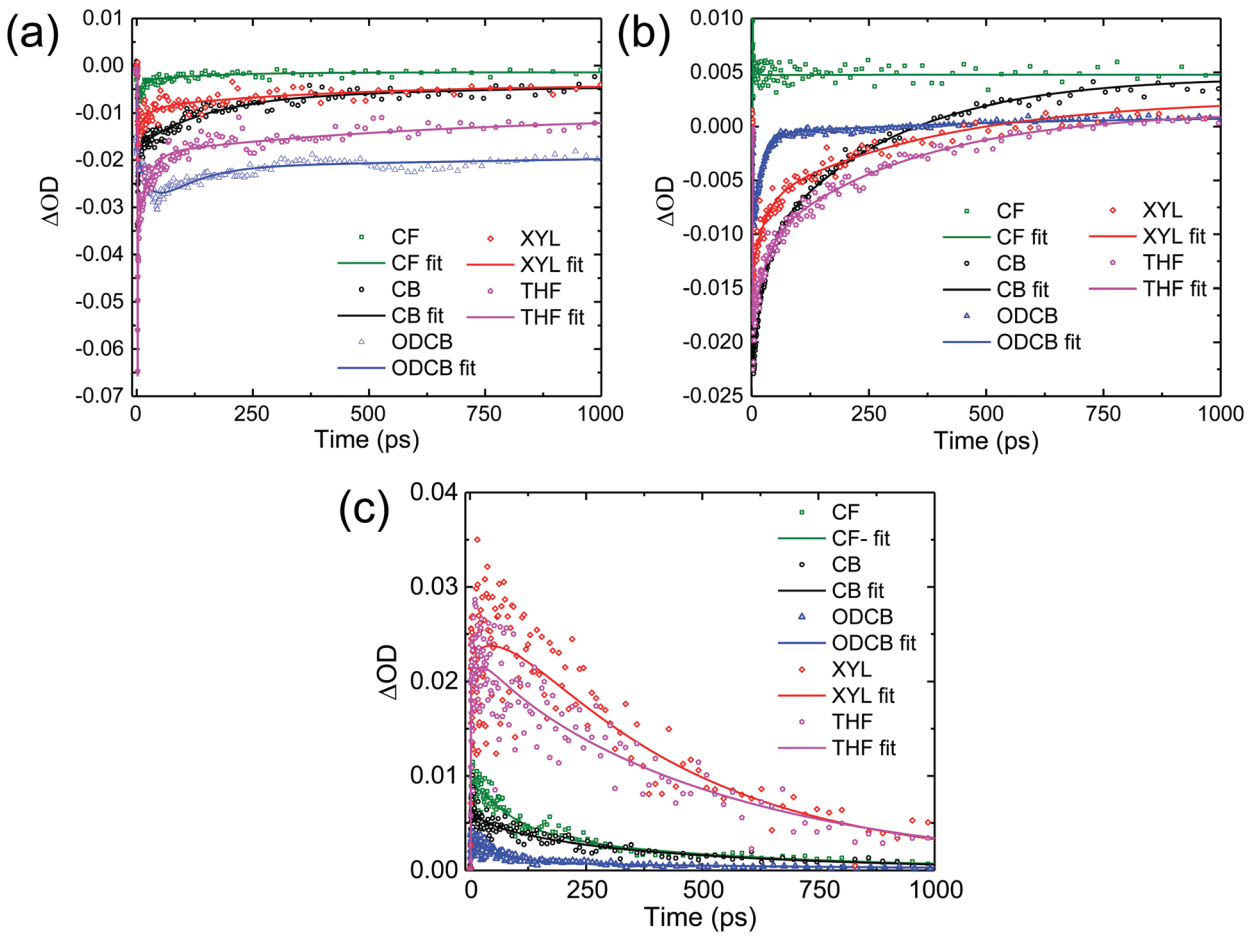

Fig. 7 Experimental TA signals (open symbols) with corresponding fits (solid lines) of the P3HT:FLR blend in different solvents as a function of pump–probe delay time: (a) GSB region (~470 nm), (b) polaron region (~600 nm), (c) singlet exciton region (~1180 nm).

Charge generation processes

To compare the charge generation by the photoinduced electron dynamics of the P3HT:FLR blend in halogenated and non-halogenated solvents, we examined their inherent kinetics. Fig. 7 shows the dynamics of the TA signals for GSB and SE (at 470 nm) and the polaron and singlet exciton absorptions (at ~600 nm and ~1180 nm, respectively) of the P3HT:FLR blend in all solvents. The fits are shown with solid colored curves. The fitting parameters used for the different probe wavelengths for the P3HT:FLR blend are shown in Table S3 (ESI†). For comparison, we have also noted the fitting parameters for pristine P3HT in all solvents (shown in Table S2, ESI†). We found GSB decays of pristine P3HT and the P3HT:FLR blend with a first ultrafast time constant (τ_1) of ~0.1 to 12 ps for all solvents (Fig. 7a). The increased polaron population depends on the decay profiles of singlet excitons. We monitored the singlet exciton decay dynamics of P3HT:FLR (Fig. 7c) and observed that the photoinduced electron transfer from D to A was fast for THF (0.739 ps) and XYL (0.133 ps) compared to halogenated solvents. This electron transfer is an order of magnitude faster than the individual exciton lifetimes of P3HT in THF (3.28 ps) and XYL (3.87 ps), respectively, indicating high efficiency of electron transfer. This can be observed by fitting the polaron region (Fig. 7b). There is a significant population of polarons for both THF (~78%) and XYL (~45%) with τ_2 ~ 27 ps, which correlates well with the PL quenching efficiency. Further, the amplitudes A1 for the faster component and A2 for the slower component have the same sign for XYL, indicating singlet exciton absorption. The amplitudes changed sign when we probed the polaron absorption, indicating a delayed increase in the polaron absorption rather than absorption decay. The variation in the long decay time (τ_3) shows the different recombination processes occurring in the system.[11,12,82] The large percentage of polarons in τ_3 suggests efficient charge generation with low recombination in the case of XYL. This type of non-radiative decay can be observed for many molecular systems.[82] Thus, from the above correlation between TAS and the optical spectroscopic conditions, one can conclude that the dissociation of excitons by addition of FLR to P3HT is enhanced for non-halogenated solvents. Upon addition of the acceptor FLR, the dissociation of excitons increased, which implies that FLR performs well as an acceptor, particularly in XYL and THF.

In the charge transfer and charge generation processes section, enhanced polarons were observed in P3HT and the P3HT:FLR blend at higher fluence energy (~16 μJ cm^{-2}) in all

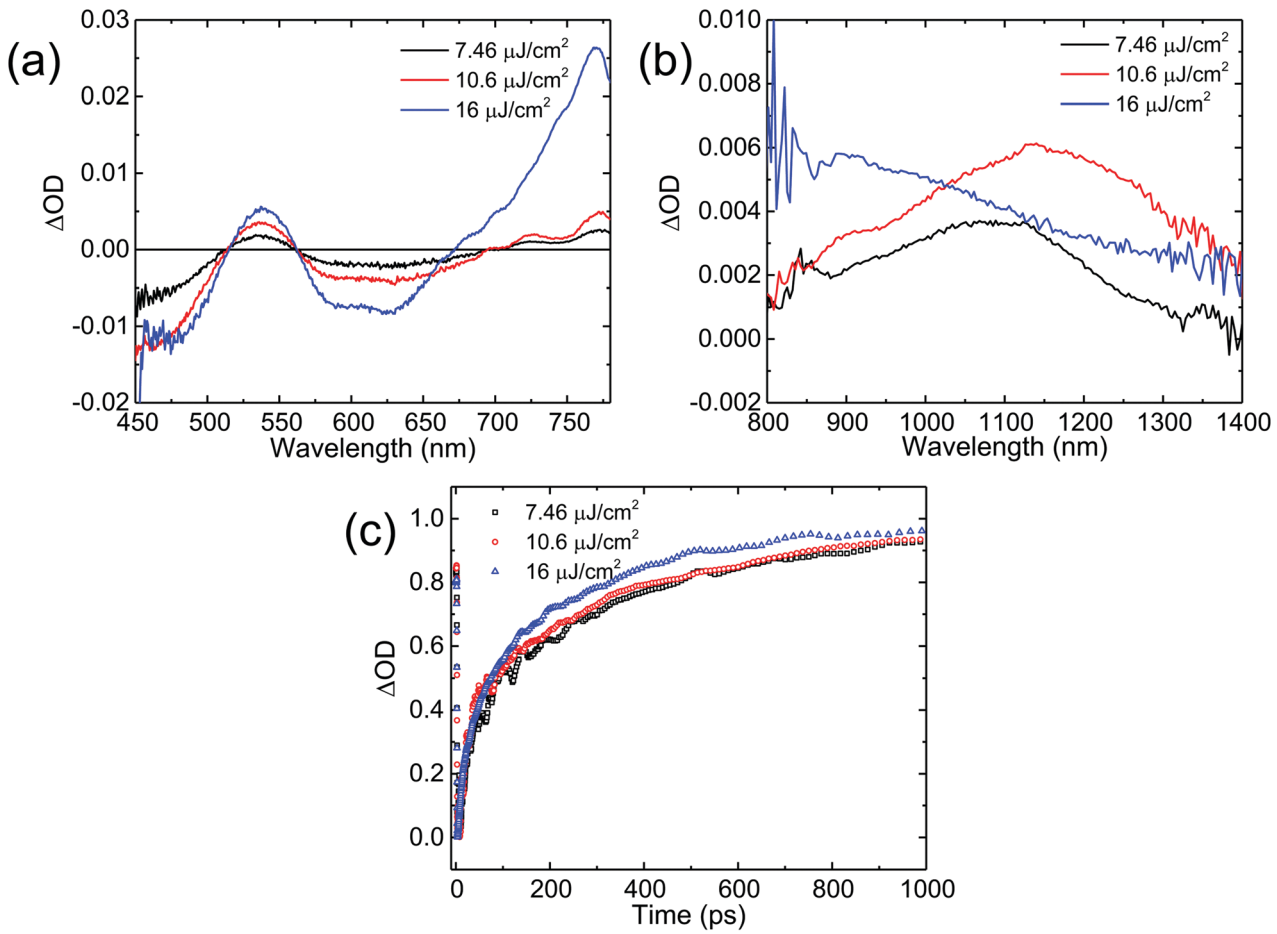

Fig. 8 TA spectra in (a) the visible region and (b) the NIR region and (c) kinetics study (excited at ~600 nm) for the P3HT:FLR blend in CB solvent at ~100 ps for different fluence energies.

the solvents; this may be due to high excited state densities *via* exciton–charge or exciton–exciton annihilation. There is a higher probability of dissociation due to these delocalized "hot exciton" charge transfer states. However, these processes are not the dominant polaron formation processes, and other processes such as recombination may also affect these states. At a higher fluence energy, the charge carrier recombination rate increases, with a corresponding enhancement in the number of polarons. Also, due to the available traps in P3HT and FLR, there is more possibility of recombination of free polarons. This can be correlated with the AFM images of the P3HT:FLR blends in different solvents, as shown in Fig. S9 (ESI†). To investigate the impact of the fluence energy on the decay dynamics, we performed TA for the P3HT:FLR blend with different fluence energies of $\sim$7.46 μJ cm^{-2}, $\sim$10.6 μJ cm^{-2} and $\sim$16 μJ cm^{-2}.

Fig. 8a and b show the TA spectra for the P3HT:FLR blend in CB solvent plotted for 100 ps in the visible and NIR regions with variable fluence energy. It can be clearly seen that with increasing fluence energy, the intensity increased in the GSB, SE and PIA regions. Fig. 8c shows a substantial increase in the decay rate with increasing fluence energy, suggesting the formation of free polarons by dissociation of excitons.[83] Considering processes such as recombination and delocalized "hot exciton" charge transfer states, we performed TA at a fluence energy of $\sim$7.46 μJ cm^{-2} for P3HT (CB and THF) and the P3HT:FLR blend for all the solvents, as shown in Fig. S7 and S8 (ESI†), respectively. To understand the charge carrier dynamics for P3HT:FLR at low fluence energy, we performed kinetic studies with excitation at $\sim$600 nm for all the solvents, as shown in Fig. 9. It can be seen that a similar trend to that for CB was observed for THF and ODCB. However, the decay rates changed for XYL and CF, suggesting the impact of fluence energy on the blend system.

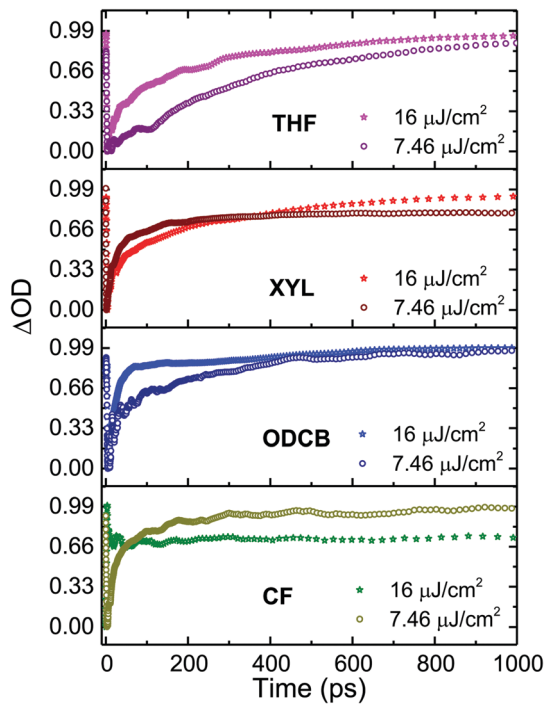

Fig. 9 Kinetics study (excited at 600 nm) of the P3HT:FLR blend in different solvents at $\sim$100 ps for fluence energies of $\sim$7.46 μJ cm^{-2} and $\sim$16 μJ cm^{-2}.

Conclusion

In essence, we describe here comprehensive studies on the influence of solvent polarity on the charge generation mechanism in a newly developed P3HT:FLR blend system using various spectroscopic tools. Based on steady-state UV-visible spectroscopy, the aggregation behavior has been revealed in this blend using different solvents. This study establishes that the degree of aggregation is associated with the exciton bandwidth and changes with the solvent polarity. The quenching behavior through photoluminescence quenching suggests that efficient charge transfer occurs between P3HT and FLR. Further, the natures of the primary photoexcitations and their dynamics were revealed for pristine P3HT and for P3HT in heterojunction with FLR in halogenated and non-halogenated solvents using vis-NIR transient absorption spectroscopy with varied probe wavelengths. Using TAS, it has been established that upon the addition of FLR to P3HT, the polaron population increased in the active layer, which shows that FLR is a promising acceptor due to efficient charge delocalization. Also, a correlation is established between the decay of the exciton population and the increase of the polaron population. This proves the formation of polarons *via* singlet exciton dissociation. It has been revealed that with varied probe wavelengths for the P3HT:FLR blend in different solvents, one can understand the influence of solvent on the exciton dissociation into free charge carriers, which can be extracted as photocurrent. In conclusion, it has been established that non-halogenated solvents such as XYL and THF generate more excitons and faster decays than halogenated solvents to dissociate efficiently into free charge carriers for the P3HT:FLR blend system.

Conflicts of interest

There are no conflicts to declare.

Acknowledgements

The authors are thankful to the Director, School of Technology, Pandit Deendayal Petroleum University (PDPU), Gujarat and the Director, CSIR-National Physical Laboratory, New Delhi for their support. The authors are thankful to Prof. Dr Rajib Bandyopadhyay, HOD, Department of Science and Prof. Nirendra Misra for their encouragement. The authors gratefully recognize the financial support from the project DST/FT/CS-120/2010, DST-EMR/2017/002252, Department of Science & Technology (DST), New Delhi, ORSP (Office of Research & Sponsored Projects), PDPU for Student Research project (ORSP/R&D/SRP/2017/SKMP), TAPSUN project funded by the Council of Scientific and Industrial Research (CSIR, NWP-54) and Indo-UK project "Advancing the effectiveness and production potential of excitonic solar cells

(APEX)''. Jessica Patel is thankful for DST-INSPIRE, Senior Research Fellowship. Dr Suresh Chand is thankful to CSIR as Emeritus Scientist and Abhishek Sharma as CSIR-RA in his emeritus scientist scheme. The authors are thankful to Dr Ritu Srivastava, Principal Scientist, Advanced Materials and Device Metrology Division, CSIR-NPL, New Delhi for providing AFM measurements.

References

1 Z. He, C. Zhong, S. Su, M. Xu, H. Wu and Y. Cao, *Nat. Photonics*, 2012, **6**, 591.
2 S. R. Scully, P. B. Armstrong, C. Edder, J. M. Fréchet and M. D. McGehee, *Adv. Mater.*, 2007, **19**, 2961–2966.
3 X. Che, Y. Li, Y. Qu and S. R. Forrest, *Nat. Energy*, 2018, **3**, 422.
4 Y. Lin and X. Zhan, *Mater. Horiz.*, 2014, **1**, 470–488.
5 M. Mojica, J. A. Alonso and F. Méndez, *J. Phys. Org. Chem.*, 2013, **26**, 526–539.
6 S. R. Dupont, M. Oliver, F. C. Krebs and R. H. Dauskardt, *Sol. Energy Mater. Sol. Cells*, 2012, **97**, 171–175.
7 Y. Lin, Y. Li and X. Zhan, *Chem. Soc. Rev.*, 2012, **41**, 4245–4272.
8 G. Zhang, J. Zhao, P. C. Chow, K. Jiang, J. Zhang, Z. Zhu, J. Zhang, F. Huang and H. Yan, *Chem. Rev.*, 2018, **118**, 3447–3507.
9 N. Liang, W. Jiang, J. Hou and Z. Wang, *Mater. Chem. Front.*, 2017, **1**, 1291–1303.
10 K. Maturová, S. S. van Bavel, M. M. Wienk, R. A. Janssen and M. Kemerink, *Nano Lett.*, 2009, **9**, 3032–3037.
11 M. Chauhan, A. Sharma, J. Patel, A. Yusuf, S. Chand, M. K. Pandey, M. Kumar, J. P. Tiwari and B. Tripathi, *Phys. Chem. Chem. Phys.*, 2018, **20**, 17304–17312.
12 A. Sharma, M. Chauhan, V. Bharti, M. Kumar, S. Chand, B. Tripathi and J. Tiwari, *Phys. Chem. Chem. Phys.*, 2017, **19**, 26169–26178.
13 H. Choi, S. J. Ko, T. Kim, P. O. Morin, B. Walker, B. H. Lee, M. Leclerc, J. Y. Kim and A. J. Heeger, *Adv. Mater.*, 2015, **27**, 3318–3324.
14 W. Zhao, D. Qian, S. Zhang, S. Li, O. Inganäs, F. Gao and J. Hou, *Adv. Mater.*, 2016, **28**, 4734–4739.
15 M. Abdelsamie, N. D. Treat, K. Zhao, C. McDowell, M. A. Burgers, R. Li, D. M. Smilgies, N. Stingelin, G. C. Bazan and A. Amassian, *Adv. Mater.*, 2015, **27**, 7285–7292.
16 Y. Sun, G. C. Welch, W. L. Leong, C. J. Takacs, G. C. Bazan and A. J. Heeger, *Nat. Mater.*, 2012, **11**, 44.
17 J. Peet, J. Y. Kim, N. E. Coates, W. L. Ma, D. Moses, A. J. Heeger and G. C. Bazan, *Nat. Mater.*, 2007, **6**, 497.
18 W. Ma, C. Yang, X. Gong, K. Lee and A. J. Heeger, *Adv. Funct. Mater.*, 2005, **15**, 1617–1622.
19 M. Campoy-Quiles, T. Ferenczi, T. Agostinelli, P. G. Etchegoin, Y. Kim, T. D. Anthopoulos, P. N. Stavrinou, D. D. Bradley and J. Nelson, *Nat. Mater.*, 2008, **7**, 158.
20 Y. Kim, S. A. Choulis, J. Nelson, D. D. Bradley, S. Cook and J. R. Durrant, *Appl. Phys. Lett.*, 2005, **86**, 063502.
21 L. Huo, T. Liu, X. Sun, Y. Cai, A. J. Heeger and Y. Sun, *Adv. Mater.*, 2015, **27**, 2938–2944.
22 J. Zhao, Y. Li, G. Yang, K. Jiang, H. Lin, H. Ade, W. Ma and H. Yan, *Nat. Energy*, 2016, **1**, 15027.
23 W. Zhao, L. Ye, S. Zhang, M. Sun and J. Hou, *J. Mater. Chem. A*, 2015, **3**, 12723–12729.
24 Y. Deng, W. Li, L. Liu, H. Tian, Z. Xie, Y. Geng and F. Wang, *Energy Environ. Sci.*, 2015, **8**, 585–591.
25 J. Y. Oh, M. Shin, T. I. Lee, W. S. Jang, Y. Min, J.-M. Myoung, H. K. Baik and U. Jeong, *Macromolecules*, 2012, **45**, 7504–7513.
26 M. J. Wirix, P. H. Bomans, M. M. Hendrix, H. Friedrich and N. A. Sommerdijk, *J. Mater. Chem. A*, 2015, **3**, 5031–5040.
27 J. H. Park, J. S. Kim, J. H. Lee, W. H. Lee and K. Cho, *J. Phys. Chem. C*, 2009, **113**, 17579–17584.
28 M. T. Dang, G. Wantz, H. Bejbouji, M. Urien, O. J. Dautel, L. Vignau and L. Hirsch, *Sol. Energy Mater. Sol. Cells*, 2011, **95**, 3408–3418.
29 T. Wang, A. D. Dunbar, P. A. Staniec, A. J. Pearson, P. E. Hopkinson, J. E. MacDonald, S. Lilliu, C. Pizzey, N. J. Terrill and A. M. Donald, *Soft Matter*, 2010, **6**, 4128–4134.
30 P. Roy, A. Jha and J. Dasgupta, *Nanoscale*, 2016, **8**, 2768–2777.
31 P. Cheng, G. Li, X. Zhan and Y. Yang, *Nat. Photonics*, 2018, **12**, 131.
32 A. J. Barker, K. Chen and J. M. Hodgkiss, *J. Am. Chem. Soc.*, 2014, **136**, 12018–12026.
33 Z. Guo, D. Lee, R. D. Schaller, X. Zuo, B. Lee, T. Luo, H. Gao and L. Huang, *J. Am. Chem. Soc.*, 2014, **136**, 10024–10032.
34 C. Zhong, H. Choi, J. Y. Kim, H. Y. Woo, T. L. Nguyen, F. Huang, Y. Cao and A. J. Heeger, *Adv. Mater.*, 2015, **27**, 2036–2041.
35 N. Banerji, *J. Mater. Chem. C*, 2013, **1**, 3052–3066.
36 J. Hou, O. Inganäs, R. H. Friend and F. Gao, *Nat. Mater.*, 2018, **17**, 119.
37 C. Yan, S. Barlow, Z. Wang, H. Yan, A. K.-Y. Jen, S. R. Marder and X. Zhan, *Nat. Rev. Mater.*, 2018, **3**, 18003.
38 A. Wadsworth, M. Moser, A. Marks, M. S. Little, N. Gasparini, C. J. Brabec, D. Baran and I. McCulloch, *Chem. Soc. Rev.*, 2019, DOI: 10.1039/c7cs00892a.
39 J. Patel, M. Chauhan, M. Aatif, A. Sharma, M. U. Trivedi, B. Tripathi, J. P. Tiwari, G. Gupta, M. Kumar and M. K. Pandey, *New J. Chem.*, 2017, **41**, 5836–5845.
40 S. Kumar, D. Kumar, Y. Patil and S. Patil, *J. Mater. Chem. C*, 2016, **4**, 193–200.
41 S. Kumar and S. Patil, *New J. Chem.*, 2015, **39**, 6351–6357.
42 Q. Yan, Y. Zhou, B.-B. Ni, Y. Ma, J. Wang, J. Pei and Y. Cao, *J. Org. Chem.*, 2008, **73**, 5328–5339.
43 L. Ding, H.-Z. Ying, Y. Zhou, T. Lei and J. Pei, *Org. Lett.*, 2010, **12**, 5522–5525.
44 G. Saranya, P. Kolandaivel and K. Senthilkumar, *J. Phys. Chem. A*, 2011, **115**, 14647–14656.
45 Y. Zhou, Y.-Z. Dai, Y.-Q. Zheng, X.-Y. Wang, J.-Y. Wang and J. Pei, *Chem. Commun.*, 2013, **49**, 5802–5804.
46 L. Ding, C. Yang, Z. Su and J. Pei, *Sci. China: Chem.*, 2015, **58**, 364–369.
47 X. Sun, Q. Xue, Z. Zhu, Q. Xiao, K. Jiang, H.-L. Yip and H. Yan, *Chem. Sci.*, 2018, **9**, 2698–2704.
48 H. Zhu, M. Li, J. Hu, X. Wang, J. Jie, Q. Guo, C. Chen and A. Xia, *Sci. Rep.*, 2016, **6**, 24313.

49 G. Li, V. Shrotriya, J. Huang, Y. Yao, T. Moriarty, K. Emery and Y. Yang, *Materials For Sustainable Energy: A Collection of Peer-Reviewed Research and Review Articles from Nature Publishing Group*, World Scientific, 2011, pp. 80–84.
50 B. Schmidt-Hansberg, M. Sanyal, M. F. Klein, M. Pfaff, N. Schnabel, S. Jaiser, A. Vorobiev, E. Müller, A. Colsmann and P. Scharfer, *ACS Nano*, 2011, **5**, 8579–8590.
51 M. Abdelsamie, K. Zhao, M. R. Niazi, K. W. Chou and A. Amassian, *J. Mater. Chem. C*, 2014, **2**, 3373–3381.
52 T. R. Andersen, T. T. Larsen-Olsen, B. Andreasen, A. P. Bottiger, J. E. Carle, M. Helgesen, E. Bundgaard, K. Norrman, J. W. Andreasen and M. Jørgensen, *ACS Nano*, 2011, **5**, 4188–4196.
53 B. J. Tremolet de Villers, K. A. O'Hara, D. P. Ostrowski, P. H. Biddle, S. E. Shaheen, M. L. Chabinyc, D. C. Olson and N. Kopidakis, *Chem. Mater.*, 2016, **28**, 876–884.
54 R. Noriega, J. Rivnay, K. Vandewal, F. P. Koch, N. Stingelin, P. Smith, M. F. Toney and A. Salleo, *Nat. Mater.*, 2013, **12**, 1038.
55 Y. Liu, J. Zhao, Z. Li, C. Mu, W. Ma, H. Hu, K. Jiang, H. Lin, H. Ade and H. Yan, *Nat. Commun.*, 2014, **5**, 5293.
56 F. Dou, E. Buchaca-Domingo, M. Sakowicz, E. Rezasoltani, T. McCarthy-Ward, M. Heeney, X. Zhang, N. Stingelin and C. Silva, *J. Mater. Chem. C*, 2015, **3**, 3722–3729.
57 J. Peet, E. Brocker, Y. Xu and G. C. Bazan, *Adv. Mater.*, 2008, **20**, 1882–1885.
58 A. L. Khan, P. Sreearunothai, L. M. Herz, M. J. Banach and A. Köhler, *Phys. Rev. B: Condens. Matter Mater. Phys.*, 2004, **69**, 085201.
59 F. Panzer, H. Bässler and A. Köhler, *J. Phys. Lett.*, 2016, **8**, 114–125.
60 F. C. Spano, *J. Chem. Phys.*, 2005, **122**, 234701.
61 J. Clark, C. Silva, R. H. Friend and F. C. Spano, *Phys. Rev. Lett.*, 2007, **98**, 206406.
62 G. Louarn, M. Trznadel, J. Buisson, J. Laska, A. Pron, M. Lapkowski and S. Lefrant, *J. Phys. Chem.*, 1996, **100**, 12532–12539.
63 J. Clark, J.-F. Chang, F. C. Spano, R. H. Friend and C. Silva, *Appl. Phys. Lett.*, 2009, **94**, 117.
64 M. Oehzelt, N. Koch and G. Heimel, *Nat. Commun.*, 2014, **5**, 4174.
65 Y. Geerts, G. Klärner and K. Müllen, *Electronic Materials: The Oligomer Approach*, 1998, pp. 1–103.
66 J. D. Lin, O. V. Mikhnenko, J. Chen, Z. Masri, A. Ruseckas, A. Mikhailovsky, R. P. Raab, J. Liu, P. W. Blom and M. A. Loi, *Mater. Horiz.*, 2014, **1**, 280–285.
67 M. E. Ziffer, S. B. Jo, H. Zhong, L. Ye, H. Liu, F. Lin, J. Zhang, X. Li, H. W. Ade and A. K.-Y. Jen, *J. Am. Chem. Soc.*, 2018, **140**, 9996–10008.
68 V. D. Mihailetchi, H. Xie, B. de Boer, L. A. Koster and P. W. Blom, *Adv. Funct. Mater.*, 2006, **16**, 699–708.
69 R. Österbacka, C. P. An, X. Jiang and Z. V. Vardeny, *Science*, 2000, **287**, 839–842.
70 X. M. Jiang, R. Österbacka, O. Korovyanko, C. P. An, B. Horovitz, R. A. Janssen and Z. V. Vardeny, *Adv. Funct. Mater.*, 2002, **12**, 587–597.
71 M. A. Stevens, C. Silva, D. M. Russell and R. H. Friend, *Phys. Rev. B: Condens. Matter Mater. Phys.*, 2001, **63**, 165213.
72 J. M. Hodgkiss, S. Albert-Seifried, A. Rao, A. J. Barker, A. R. Campbell, R. A. Marsh and R. H. Friend, *Adv. Funct. Mater.*, 2012, **22**, 1567–1577.
73 J. Cornil, D. Beljonne, J. P. Calbert and J. L. Brédas, *Adv. Mater.*, 2001, **13**, 1053–1067.
74 O. F. Mohammed, *J. Phys. Chem. A*, 2010, **114**, 11576–11582.
75 I. A. Howard, R. Mauer, M. Meister and F. Laquai, *J. Am. Chem. Soc.*, 2010, **132**, 14866–14876.
76 A. Köhler and H. Bässler, *Mater. Sci. Eng., R*, 2009, **66**, 71–109.
77 S. Westenhoff, W. J. Beenken, R. H. Friend, N. C. Greenham, A. Yartsev and V. Sundström, *Phys. Rev. Lett.*, 2006, **97**, 166804.
78 J. Piris, T. E. Dykstra, A. A. Bakulin, P. H. V. Loosdrecht, W. Knulst, M. T. Trinh, J. M. Schins and L. D. Siebbeles, *J. Phys. Chem. C*, 2009, **113**, 14500–14506.
79 B. S. Rolczynski, J. M. Szarko, H. J. Son, Y. Liang, L. Yu and L. X. Chen, *J. Am. Chem. Soc.*, 2012, **134**, 4142–4152.
80 O. P. Dimitriev, D. A. Blank, C. Ganser and C. Teichert, *J. Phys. Chem. C*, 2018, **122**, 17096–17109.
81 N. Banerji, J. Seifter, M. Wang, E. Vauthey, F. Wudl and A. J. Heeger, *Phys. Rev. B: Condens. Matter Mater. Phys.*, 2011, **84**, 075206.
82 D. Herrmann, S. Niesar, C. Scharsich, A. Köhler, M. Stutzmann and E. Riedle, *J. Am. Chem. Soc.*, 2011, **133**, 18220–18233.
83 M. A. Alamoudi, J. I. Khan, Y. Firdaus, K. Wang, D. Andrienko, P. M. Beaujuge and F. D. R. Laquai, *ACS Energy Lett.*, 2018, **3**, 802–811.

